Available online at www.sciencedirect.com
ScienceDirect
Journal of the European Ceramic Society 28 (2008) 2557–2562
www.elsevier.com/locate/jeurceramsoc

Investigation into the interactions between Bi_2O_3-doped ZnO and AgPd electrode

Shu-Ting Kuo [a], Wei-Hsing Tuan [a,*], Yeh-Wu Lao [b], Chung-Kai Wen [b], Huey-Ru Chen [b], Hsin-Yi Lee [c]

[a] *Department of Materials Science and Engineering, National Taiwan University, Taipei 106, Taiwan*
[b] *Walsin Technology Corporation, Kaohsiung 700, Taiwan*
[c] *National Synchrotron Radiation Research Center, Hsinchu 300, Taiwan*

Received 5 January 2008; received in revised form 10 March 2008; accepted 20 March 2008
Available online 19 May 2008

Abstract

Bi_2O_3-doped ZnO multilayer specimens with inner AgPd electrodes are prepared. The interactions between the Bi_2O_3 dopants and AgPd electrodes at elevated temperatures are investigated. It is found that during co-firing, two oxide phases, PdO and $PdBi_2O_4$, are formed at 400 °C and 600 °C, respectively, using synchrotron X-ray analysis. The $PdBi_2O_4$ phase remains in the multilayer specimens after co-firing. Despite the formation of $PdBi_2O_4$, the Pd content in the AgPd electrodes increases with increasing firing temperature. In contrast, a decrease in Ag content in the electrodes at elevated temperatures is apparent; this is mainly due to the vaporization of Ag. The present study shows that after firing at 1200 °C for 1 h, the inner AgPd electrodes experience degradation due to the formation of $PdBi_2O_4$ and the loss of Ag.

Keywords: ZnO; Varistor; Microstructure-final; Firing; Multilayer

1. Introduction

Many passive components nowadays are in multilayered structure due to the demands on miniaturization and integration. In order to increase the volume efficiency, the layer thickness is decreasing from ten of micrometers to several micrometers in the last decade.[1–2] The interactions between ceramic layers and inner electrodes become important for the performance of multilayered components.

The ZnO-based ceramics exhibit unique nonlinear current–voltage (*I–V*) characteristics; they are commonly used as the varistors to protect electronic devices against voltage surges.[3–5] Recently, multilayer varistors (MLV) have been developed for low voltage applications. Though many metal oxides have been used as additives for ZnO-based varistors, Bi_2O_3 carries a special importance since it enhances the grain growth and affects the stability of the nonlinear *I–V* characteristics.[3,5–7] Though precious metal Pt has been proved as a suitable material for the inner electrodes for ZnO-based MLV,[8] AgPd alloys are now considered as candidate materials for the inner electrode due to the cost issue.

The basic requirement on the inner electrode is its ability to co-fire with ZnO-based ceramics at elevated temperatures. Previous studies on multilayer ceramic capacitor (MLCC) systems indicated that reactions could take place between AgPd and Bi_2O_3.[9–11] For example, pure Pd could react with Bi_2O_3 to form $PdBi_2O_4$.[10] However, the reaction phase $PdBi_2O_4$ is not stable at elevated temperatures.[9] Hrovat et al. also indicated that AgPd could react with $Bi_2Ru_2O_7$ to form a solid solution of Bi and Pd.[12] Since Bi_2O_3 is usually added to ZnO-based varistors, the interaction between Bi_2O_3 and AgPd alloys at elevated temperature is a topic of increasing technological importance.

In the present study, a model varistor composition, 5 wt% Bi_2O_3-doped ZnO, is used as the ceramic part. A co-precipitated AgPd (70 wt%/30 wt%) powder is used as the inner electrode. The metallic electrodes and seven ceramic layers of various thicknesses are laminated into a multilayer structure. The phase and microstructure evolution during co-firing are then investigated.

* Corresponding author. Tel.: +886 2 33663899.
E-mail address: tuan@ntu.edu.tw (W.-H. Tuan).

0955-2219/$ – see front matter © 2008 Elsevier Ltd. All rights reserved.
doi:10.1016/j.jeurceramsoc.2008.03.036

2. Experimental

To prepare the 5 wt% Bi_2O_3 doped ZnO green tape, several solvents and binders were first mixed with ceramic powders. The tape of a thickness of 20 μm was then cast. A 70%Ag–30%Pd co-precipitate powder was used for inner electrode. The Ag/Pd paste was deposited onto the green tape by screen printing. A multilayer structure containing seven layers with thicknesses varying from 20 μm to 140 μm was made by laminating different numbers of green tapes. To facilitate the comparison, the layers with different thicknesses were all built into one component. The cross-section of one typical multilayer specimen is shown in Fig. 1(a). The laminates were then cut into a size of 1.85 mm (length) × 0.95 mm (width) × 0.75 mm (thickness). All specimens were firstly fired from room temperature to 400 °C in air for 1 h using a heating rate of 1 °C/min to remove the organics. After the binder burnout stage, the firing was performed in air at 600 °C to 1200 °C for 60 min, with the heating and cooling rates of 5 °C/min. In order to prevent the vaporization of Bi_2O_3 at elevated temperatures,[13] the specimens were sintered in a powder bed composed of ZnO and 5 wt% Bi_2O_3.

Several bulk specimens with the diameter of 10 mm and thickness of 3 mm were also prepared for comparison. The composition of the bulk specimen was ZnO, 5 wt% Bi_2O_3 and 15 wt% AgPd. A powder bed was also used during firing; its composition is the same as that of the bulk specimens. For microstructure observation, the specimens were ground with SiC abrasive papers and polished with 0.05 μm Al_2O_3 particles. The specimens were etched with dilute hydrochloric acid. The microstructures were observed by a scanning electron microscopy (SEM, XL-30, Philips Co., Netherlands). The composition analyses were carried out by using an electron probe microanalysis (EPMA, Model JAX-8200, JOEL, Japan). The phases of sintered bulk and multilayer specimens were characterized with a synchrotron X-ray (Beam line 17B1, National Synchrotron Radiation Research Center, Hsinchu, Taiwan). Incident X-rays were focused vertically with a mirror and made monochromatic at energy of 8 keV with a Si (1 1 1) double-crystal monochromator; the sagittal bend of the second crystal focused the X-rays in the horizontal direction. With two pairs of slits between the specimen and the detector, the typical scattering vector resolution in the vertical scattering plane was $\sim 5 \times 10^{-3}$ nm^{-1}. In order to carry out the phase analysis on multilayer specimens, several multilayer specimens were mounted together into resin then ground to expose the cross section of the specimens. The synchrotron X-ray beam was then spotted at the cross section of the specimens to carry out the phase analysis.

3. Results

3.1. ZnO–Bi_2O_3/AgPd multilayer specimens

Fig. 1 shows the cross-sections of typical multilayer specimens of Bi_2O_3-doped ZnO and AgPd inner electrodes after sintering at 1100 °C and 1200 °C in air for 60 min. The thickness of the Bi_2O_3-doped ZnO layer varies from 8 μm to 55 μm after sintering at 1100 °C for 60 min, Fig. 1(a). As the multilayer specimen is sintered at 1200 °C for 60 min, most the AgPd electrodes no longer existed at their original place, Fig. 1(b). Large holes were formed instead. The thickness of the remaining AgPd electrode becomes thicker. Fig. 2 shows a typical microstructure near the remaining AgPd electrodes after sintering at 1200 °C for 60 min. The corresponding EPMA results are shown in Table 1. From the EPMA analysis, the composition of point "a" includes Ag and Pd elements and a small amount of Bi and Zn elements.

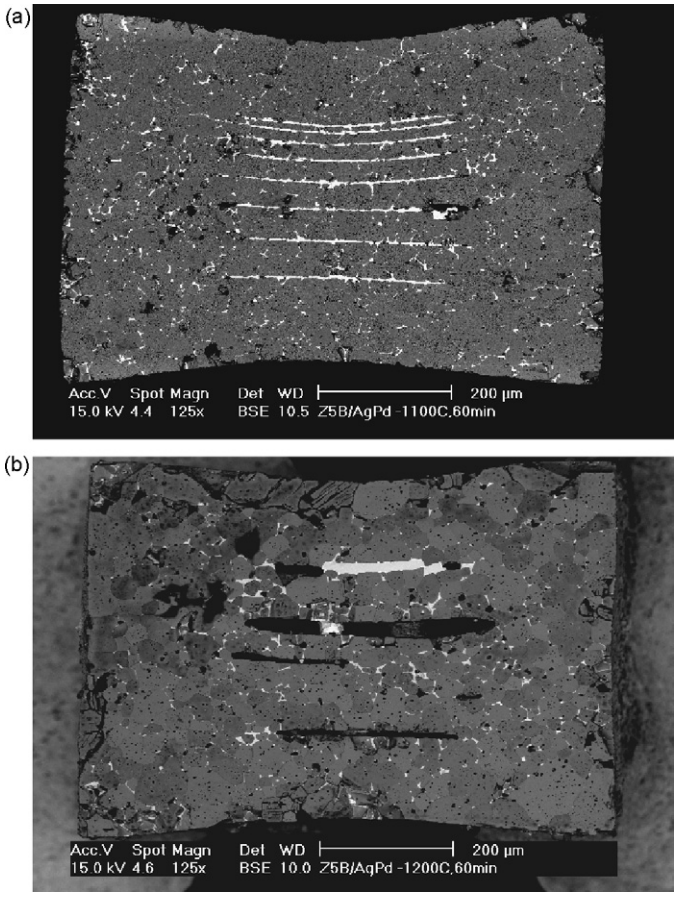

Fig. 1. Cross-sections of Bi_2O_3-doped ZnO/AgPd multilayer specimens after sintering at (a) 1100 °C and (b) 1200 °C for 60 min.

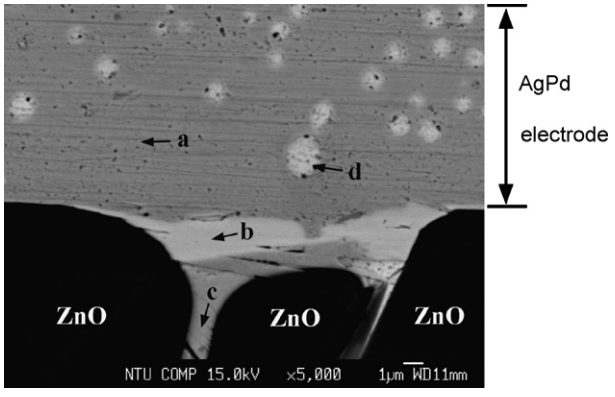

Fig. 2. SEM micrograph of a multilayer specimen after sintering at 1200 °C for 60 min. The EPMA results for a, b, c and d points can be found in Table 1.

Table 1
EPMA results for the multilayer specimen shown in Fig. 2

Element (at%)	Position			
	Point a	Point b	Point c	Point d
Bi	5.2	34.4	32.3	38.9
O	–	44.2	51.0	48.3
Ag	29.3	0.8	1.1	4.2
Pd	62.3	14.8	–	4.2
Zn	3.2	5.8	15.6	4.3
Phase	AgPd	$PdBi_2O_4$	Bi_2O_3-rich phase	Bi_2O_3-rich phase

Point "a" is thus identified as AgPd electrode. Point "b" for the phase with platelet shape mainly consists of Pd, Bi, and O elements. The amounts of Ag and Zn in the phase are small. The ratio between Pd, Bi, and O elements is close to 1:2:4, suggesting that the phase is a $PdBi_2O_4$. Regarding point "c", it locates at the ZnO/ZnO grain boundary. The composition is mainly Bi and O, and a relatively small amount of Zn element. Since an amount of 25 mol% of ZnO is needed to dissolve into Bi_2O_3 to form an eutectic liquid;[14–17] the phase of point "c" is therefore a Bi_2O_3–ZnO eutectic phase. The eutectic phase is termed as Bi_2O_3-rich phase in the following text. Some spherical particles, point "d", are found embedded within AgPd electrode. The composition is mainly Bi and O; the amounts of Ag, Pd, and Zn are low. It suggests that the phase of point "d" is also a Bi_2O_3-rich phase.

Fig. 3 shows the synchrotron X-ray patterns for the Bi_2O_3-doped ZnO/AgPd multilayer specimens after sintering at various temperatures. The X-ray pattern for the specimen after binder burnout at 400 °C is shown for comparison purpose. The XRD pattern reveals the presence of ZnO, Bi_2O_3 and AgPd in the specimen after binder burnout. The peaks for pure Ag and pure Pd are not found, indicating that the AgPd alloy is formed after firing at 400 °C for 1 h. Thanks to the sensitivity of the synchrotron X-ray source, a very small amount of PdO is detected. It indicates that the oxidation of Pd has taken place below 400 °C. The oxidation product of the AgPd alloy, PdO, decreases in its amount in the temperature range from 400 °C to 700 °C. As the temperature increases to 700 °C, a new phase $PdBi_2O_4$ is formed through the consumption of PdO. In the temperature range from 800 °C to 1200 °C, ZnO, Bi_2O_3-rich phase, AgPd and $PdBi_2O_4$ are present, whereas PdO is no longer found. The phases formed

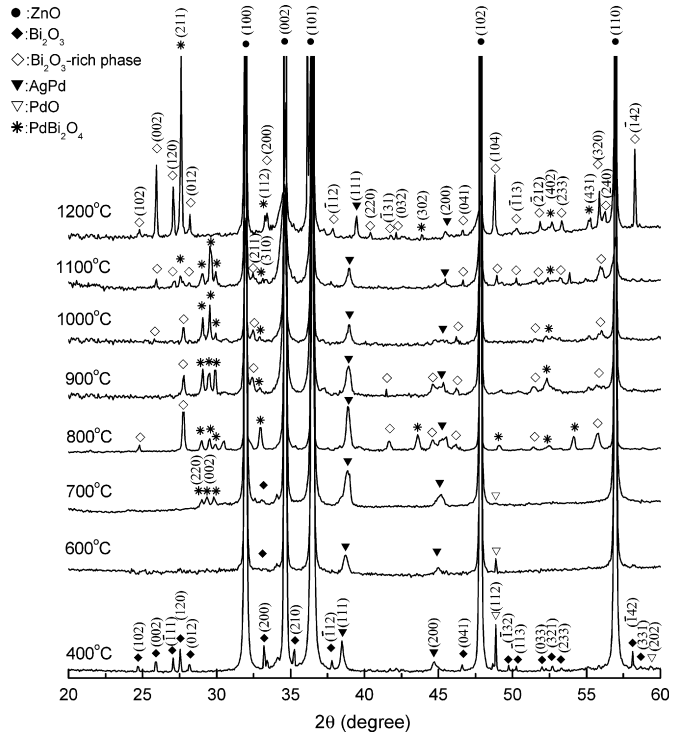

Fig. 3. XRD patterns for the ZnO–Bi_2O_3/AgPd multilayer specimens sintered at the indicated temperatures for 60 min.

after firing at the indicated temperatures are shown in Table 2. In addition, the AgPd (1 1 1) and (2 0 0) peaks shift to higher angles with increasing sintering temperature, indicating that the lattice parameters decrease with increasing firing temperature. Using these two characteristic peaks, the lattice parameter, *a*, of AgPd alloy can also be calculated. Fig. 4 shows the lattice parameter of AgPd alloy as a function of sintering temperature. The lattice parameter of AgPd decreases rapidly from 4.05 Å to 3.97 Å with the increase of firing temperature from 400 °C to 1200 °C.

3.2. *ZnO–Bi_2O_3–AgPd bulk specimens*

The Bi_2O_3-doped ZnO and AgPd particles are thoroughly mixed in the bulk specimens. Fig. 5 shows the typical micrograph of the ZnO–5 wt% Bi_2O_3–15 wt% AgPd bulk specimens. The Bi_2O_3-rich phase mainly locates at the grain boundaries between

Table 2
Phases found in the multilayer and bulk specimens after sintering at the indicated temperatures for 60 min

Temperature (°C)	Multilayer specimen	Bulk specimen
Room temperature	ZnO, Bi_2O_3, Ag/Pd*	ZnO, Ag/Pd*, Bi_2O_3
400 °C	ZnO, Bi_2O_3, AgPd, PdO	ZnO, AgPd, Bi_2O_3, PdO
600 °C	ZnO, AgPd, PdO, Bi_2O_3	ZnO, AgPd, Bi_2O_3, $PdBi_2O_4$, PdO
700 °C	ZnO, AgPd, $PdBi_2O_4$, Bi_2O_3, PdO	ZnO, AgPd, Bi_2O_3, $PdBi_2O_4$, PdO
800 °C	ZnO, AgPd, $PdBi_2O_4$, Bi_2O_3-rich phase	ZnO, AgPd, $PdBi_2O_4$, Bi_2O_3-rich phase
900 °C	ZnO, AgPd, $PdBi_2O_4$, Bi_2O_3-rich phase	ZnO, AgPd, $PdBi_2O_4$, Bi_2O_3-rich phase
1000 °C	ZnO, AgPd, $PdBi_2O_4$, Bi_2O_3-rich phase	ZnO, AgPd, $PdBi_2O_4$, Bi_2O_3-rich phase
1100 °C	ZnO, $PdBi_2O_4$, AgPd, Bi_2O_3-rich phase	ZnO, AgPd, $PdBi_2O_4$, Bi_2O_3-rich phase
1200 °C	ZnO, $PdBi_2O_4$, Bi_2O_3-rich phase, AgPd	ZnO, AgPd, $PdBi_2O_4$, Bi_2O_3-rich phase

The amount of the phases in each specimen decreases from the left-hand side to the right-hand side.
Note: *Ag/Pd = Ag and Pd co-precipitated powder, AgPd = AgPd alloy.

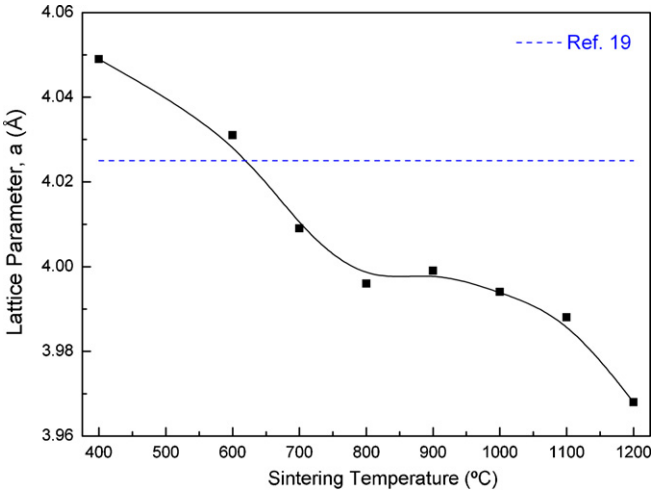

Fig. 4. Lattice parameter of the AgPd alloys in multilayer specimens as a function of sintering temperature. The reported value[19] for the 70Ag30Pd is also shown for comparison.

ZnO grains. The AgPd particles exist both at the boundary sites and within ZnO grains. As the addition of Bi_2O_3 reduces the grain boundary energy,[18] the mobility of grain boundaries is high. They move easily through the ZnO grains and leave behind many AgPd particles.

The synchrotron XRD patterns of the bulk specimens are shown in Fig. 6. Similar to the multilayer specimens, the PdO phase is also found in the specimen after firing at 400 °C for 1 h. The reaction phase, $PdBi_2O_4$, is found after firing at 600 °C for 1 h, which is 100 °C lower than that in the multilayer specimen. The PdO and $PdBi_2O_4$ co-existed between 600 °C to 700 °C. Above 800 °C, the $PdBi_2O_4$ remains in the bulk specimens after sintering. The lattice parameter of AgPd alloy also decreases with the increase of sintering temperature. The lattice parameters of the AgPd alloy in the bulk specimens, shown in Fig. 7, differ from the multilayer specimens; the lattice parameter of the AgPd alloy in bulk specimens has not decreased further as the sintering temperature is higher than 700 °C.

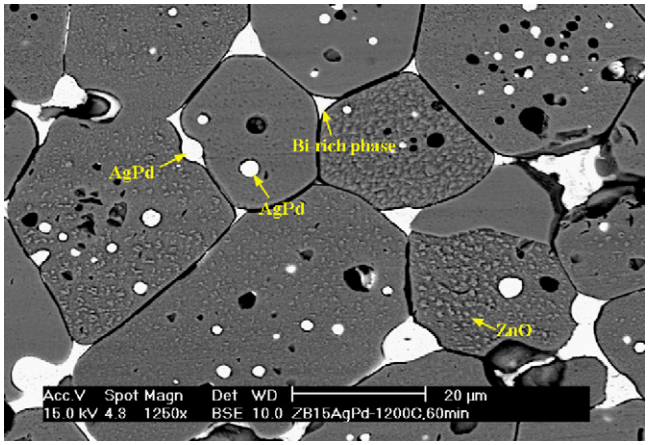

Fig. 5. Microstructure of the ZnO–Bi_2O_3–AgPd bulk specimen after sintering at 1200 °C for 60 min.

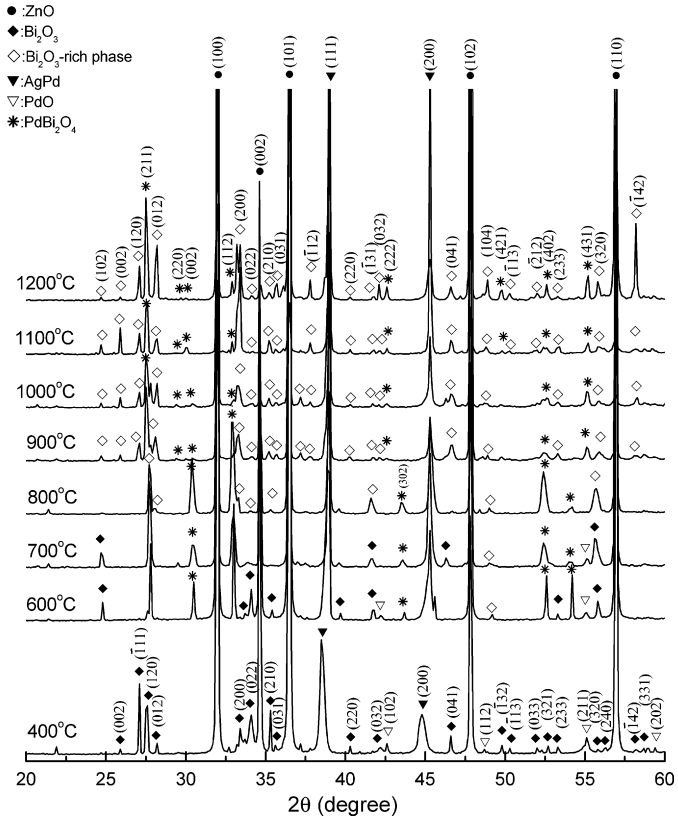

Fig. 6. XRD patterns for the ZnO–Bi_2O_3–AgPd bulk specimens sintered at the indicated temperatures for 60 min.

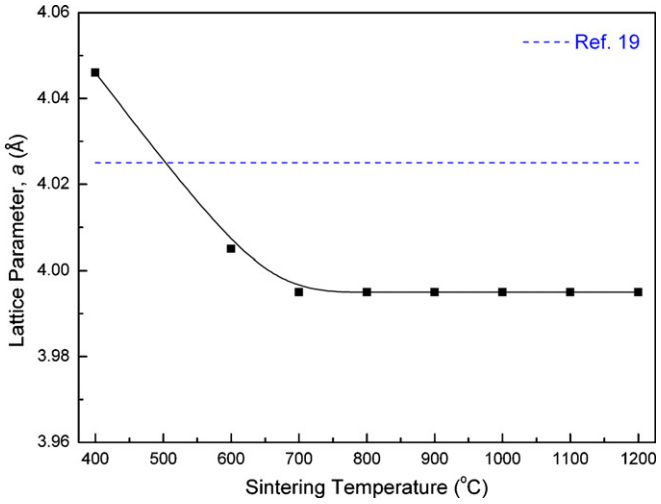

Fig. 7. Lattice parameter of the AgPd alloys in bulk specimens as a function of sintering temperature. The reported value[19] for the 70Ag30Pd is also shown for comparison.

4. Discussion

In the present study, the ZnO–Bi_2O_3/AgPd multilayer and ZnO–Bi_2O_3–AgPd bulk specimens are prepared. In the bulk specimens, the ZnO, Bi_2O_3 particles mixed intimately with the AgPd particles. The reactions, if any, between ZnO, Bi_2O_3 and AgPd would take place during sintering at elevated temperature. The reaction phase, $PdBi_2O_4$, is formed in the bulk specimen

at a temperature as low as 600 °C. The reaction phase locates between the Bi_2O_3-rich liquid phase and AgPd, Fig. 2, indicating that the phase is indeed the reaction product of the Bi_2O_3 and AgPd. Except the early formation of $PdBi_2O_4$ in the bulk specimen, the XRD patterns of the bulk specimens are similar to those of the multilayer specimens. It demonstrates that Bi_2O_3-doped ZnO layer could react with AgPd electrode during co-firing at a temperature above 600 °C.

The melting point of 70Ag–30Pd alloy is around 1200 °C.[10,19] The alloy is frequently used as the inner electrode for many multilayer components.[1,10] The melting point of Bi_2O_3–ZnO eutectic is 740 °C.[5,17] The oxidation of AgPd starts from a temperature below 400 °C. The oxidation product PdO then starts to decompose above 400 °C. No PdO is found in the specimen as the firing temperature is higher than 800 °C. The formation of $PdBi_2O_4$ consumes some of the Bi_2O_3-rich liquid phase. The amount of $PdBi_2O_4$ increases as the Bi_2O_3–ZnO eutectic liquid is formed. Furthermore, the intensity of the $PdBi_2O_4$ (0 0 2) peak is the highest below 800 °C, then the $PdBi_2O_4$ (2 1 1) peak is the highest above 900 °C. The temperature range roughly corresponds to the formation of the Bi_2O_3-rich liquid phase, indicating a texture for the reaction phase $PdBi_2O_4$ is formed through the assistance of the Bi_2O_3-rich liquid phase.

From the XRD analyses, the following reactions have taken place during the co-firing of Bi_2O_3-doped ZnO and AgPd. Below 400 °C, the Ag/Pd co-precipitated powder forms AgPd alloy first. Previous study on the interdiffusion between Ag and Pd thin films also indicated that the AgPd alloy is formed after firing at 450 °C for 40 s[20] as

$$\frac{Ag}{Pd_{(s)}} \rightarrow AgPd_{(s)} \quad (1)$$

Then, the oxidation of the AgPd alloy has taken place, as

$$AgPd_{(s)} + \tfrac{1}{2}O_2 \rightarrow PdO_{(s)} + AgPd_{(s)} \quad (2)$$

At a temperature above 400 °C, PdO is decomposed to form Pd then to dissolve into AgPd alloy as;

$$PdO_{(s)} \rightarrow Pd_{(s)} + \tfrac{1}{2}O_{2(s)} \quad (3)$$

$$Pd_{(s)} + AgPd_{(s)} \rightarrow AgPd_{(s)} \quad (4)$$

The PdO can also react with Bi_2O_3 to form $PdBi_2O_4$, as

$$PdO + Bi_2O_{3(s)} \rightarrow PdBi_2O_4 \quad (5)$$

Above 800 °C, the amount of $PdBi_2O_4$ is increased without the presence of PdO. To be demonstrated later, part of the Ag in the AgPd alloy is vaporized, as

$$AgPd_{(s)} \rightarrow AgPd_{(s)} + Ag_{(g)} \quad (6)$$

Previous studies indicated that both PdO and $PdBi_2O_4$ are not stable above 900 °C.[10,11] The decomposition temperature of $PdBi_2O_4$ is around 35 °C higher than that of PdO.[10] It is thus likely that the PdO is formed first during the cooling stage. The PdO is then reacted with the Bi_2O_3 to form $PdBi_2O_4$. In the present study, a very large amount of powder bed is used to surround each specimen. There is 5 wt% Bi_2O_3 in the powder bed. The evaporation of Bi_2O_3 is therefore suppressed. The presence of Bi_2O_3 encourages the formation of $PdBi_2O_4$. The reaction phase $PdBi_2O_4$ is therefore found in the specimens after sintering.

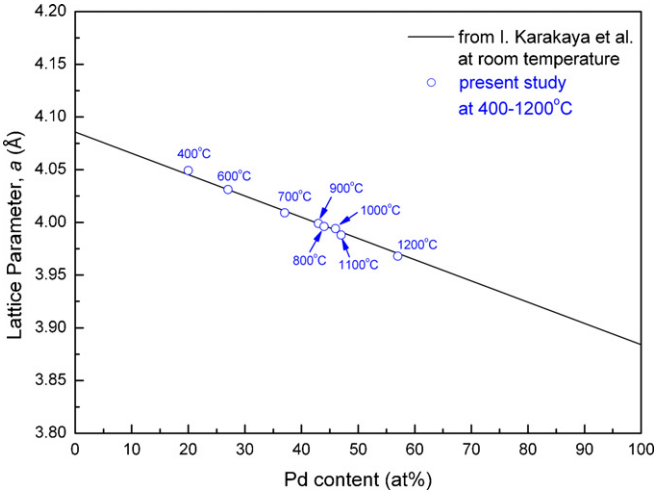

Fig. 8. Lattice parameters of AgPd alloys in the multilayer specimens as a function of Pd content. The solid line is proposed by Karakaya and Thompson.[19]

In the present study, the lattice parameter of AgPd alloy is used to determine the composition of AgPd inner electrode. The crystal structure of Ag and Pd is the same, face centered cubic. The lattice parameter of Ag and Pd atoms is 1.44 Å and 1.37 Å, respectively.[9,19] The Ag atom can easily substitute Pd atom in the lattice and vice versa. Fig. 8 shows the correlation between the lattice parameter of AgPd alloys and Pd content for the multilayer specimens. A straight line for the lattice parameter of AgPd alloys as proposed by Karakaya and Thompson[19] is also shown in the figure. The lattice parameter of the AgPd alloys follows the straight line with the Pd content. From the straight line, the composition of AgPd alloy after firing at various temperatures can therefore be estimated. The results are shown in Table 3. At the temperature below 700 °C, the Pd content is lower than 30%, it can be related to the formation of PdO. As the temperature is higher than 700 °C, the formation of $PdBi_2O_4$ further consumes the Pd from the inner electrode. Nevertheless, the amount of Ag in the electrode decreases with the increase of sintering temperature.

Table 3
Composition of AgPd alloys as determined from their lattice parameters

Temperature (°C)	Composition (at%)	
	Multilayer	Bulk
400	80Ag/20Pd	81Ag/19Pd
600	73Ag/27Pd	60Ag/40Pd
700	63Ag/37Pd	55Ag/45Pd
800	56Ag/44Pd	55Ag/45Pd
900	57Ag/43Pd	55Ag/45Pd
1000	54Ag/46Pd	55Ag/45Pd
1100	53Ag/47Pd	55Ag/45Pd
1200	43Ag/57Pd	55Ag/45Pd

The vapor pressure of Ag is relatively high at elevated temperature (ex. 0.2 mmHg at 1200 °C),[21] it is easily vaporized during firing. During the firing of the ZnO–Bi_2O_3–AgPd bulk specimens, a powder bed with the same composition is also used. By using such Ag-containing powder bed the lattice parameter of the AgPd alloy is not decreased above 900 °C, Fig. 7. It confirms that the vaporization of Ag from AgPd electrode has indeed taken place during firing. Furthermore, it also suggests that the loss of Ag through vaporization can be suppressed by using a suitable powder bed.

Two processes are competing with each other at elevated temperatures, one process involves the consumption of Pd from inner electrode to form PdO and $PdBi_2O_4$, and the other one involves the vaporization of Ag. The oxidation of Pd has taken place below 600 °C. The amount of Ag is less than 70% after firing above 700 °C. The vapor pressure of Ag at a temperature below its melting point is low (less than 10^{-5} mmHg at 700 °C)[21]. The decrease of Ag amount in the AgPd alloy below 700 °C needs further investigation. The amount of $PdBi_2O_4$ increases with the increase of firing temperature, so does the vaporization of Ag. The X-ray intensity of AgPd peaks in the multilayer specimens decreases dramatically above 1200 °C, Fig. 3. It indicates that the extent of both reactions increases with the increase of temperature. As a result, the amount of AgPd alloy is significantly decreased above 1200 °C, Fig. 1(b). Therefore, the inner electrode is no longer continuous in the multilayer specimens. The integrity of the inner electrodes is lost as the multilayer specimen is fired at 1200 °C for 60 min.

5. Conclusions

In the present study, the feasibility of using metallic AgPd as the inner electrodes for multilayer varistors (MLV) is evaluated. The composition of the AgPd phase after firing is determined by using a high resolution X-ray analysis. Through the usage of a powder bed, the Bi_2O_3 remains in the specimen during cooling stage. The amount of Pd in AgPd alloy is decreased due to the formation of $PdBi_2O_4$. The vaporization of Ag reduces the amount of Ag in the electrode. The composition of AgPd alloy is therefore a function of firing temperature. Due to these reactions, the AgPd electrodes are no longer continuous in the multilayer specimen after firing at 1200 °C for 60 min. It thus demonstrates that there is a temperature limit for the firing of MLV when an AgPd alloy is used as the inner electrode.

References

1. Kishi, H., Mizuno, Y. and Chazono, H., Base-metal electrode-multilayer ceramic capacitors: past, present and future perspectives. *Jpn. J. Appl. Phys.*, 2003, **42**(1), 1–15.
2. Pepin, J. G., Borland, W., O'Callaghan, P. and Young, R. J. S., Electrode-based causes of delaminations in multilayer ceramic capacitors. *J. Am. Ceram. Soc.*, 1989, **72**(12), 2287–2291.
3. Gupta, T. K., Application of zinc oxide varistors. *J. Am. Ceram. Soc.*, 1990, **77**(7), 1817–1840.
4. Levinson, L. M. and Philips, H. R., Zinc oxide varistor—a review. *Ceram. Bull.*, 1986, **65**(4), 639–646.
5. Clarke, D. R., Varistor creamics. *J. Am. Ceramic. Soc.*, 1999, 82, 485–502.
6. Einzinger, R., Metal oxide varistors. *Annu. Rev. Mater. Sci.*, 1987, **17**, 299–321.
7. Matsuoka, M., Non-ohmic properties of zinc oxide ceramic. *Jpn. J. Appl. Phys.*, 1971, **10**, 736–746.
8. Kuo, S. T., Tuan, W. H., Lao, Y. W., Wen, C. K. and Chen, H. R., Grain growth behavior of Bi_2O_3-doped ZnO grains in multilayer varistor. *J. Am. Ceram. Soc.*, in press.
9. Wang, S. F. and Huebner, W., Thermodynamic modeling of equilibrium subsolidus phase relations in the Ag–Pd–O_2 system. *J. Am. Ceram. Soc.*, 1991, **74**(6), 1349–1353.
10. Wang, S. F. and Huebner, W., Interaction of Ag/Pd metallization with lead and bismuth oxide-based fluxes in multilayer ceramic capacitors. *J. Am. Ceram. Soc.*, 1992, **75**(9), 2339–2352.
11. Wang, S. F. and Huebner, W., Interaction of silver/palladium electrodes with lead- and bismuth-based electroceramics. *J. Am. Ceram. Soc.*, 1993, **76**(2), 474–480.
12. Hrovat, M., Jan, F. and Kolar, D., The interactions between thick film conductors and low ohmic resistors. *Hybrid Circuits*, 1986, **10**(1), 14–15.
13. Lao, Y. W., Kuo, S. T. and Tuan, W. H., Effect of powder bed on the microstructure and electrical properties of Bi_2O_3- and Sb_2O_3-doped ZnO. *J. Mater. Sci. Mater.* Electron., in press.
14. Miles, G. C. and West, A. R., Pyrochlore phase in the system ZnO–Bi_2O_3–Sb_2O_3. I. Stoichiometries and phase equilibria. *J. Am. Ceram. Soc.*, 2006, **89**(3), 1042–1046.
15. Lee, J. R., Chiang, Y. M. and Ceder, G., Pressure-thermodynamic study of grain boundaries: Bi segregation in ZnO. *Acta Metall. Mater.*, 1997, **45**(3), 1247–1257.
16. Luo, J., Wang, H. and Chiang, Y. M., Origin of solid-state activated sintering in Bi_2O_3-doped ZnO. *J. Am. Ceram. Soc.*, 1999, **82**(4), 916–920.
17. de la Rubia, M. A., Fernandez, J. F. and Caballero, A. C., Equilibrium phases in the Bi_2O_3-rich region of the ZnO–Bi_2O_3 system. *J. Eur. Ceram. Soc.*, 2005, **25**, 2215–2217.
18. Wang, H. and Chiang, Y. M., Thermodynamic stability of intergranular amorphous films in bismuth-doped zinc oxide. *J. Am. Ceram. Soc.*, 1998, **81**(1), 89–96.
19. Karakaya, I. and Thompson, W. T., The Ag/Pd system. *Bull. Alloy Phase Diag.*, 1988, **9**(3), 237–243.
20. Baither, D., Kim, T. H. and Schmitz, G., Diffusion-induced recrystallization in silver–palladium layers. *Scr. Mater.*, 2008, **58**(1), 99–102.
21. Metal Handbook, vol. 1. Am. Soc. For Metals, Metal Park, OH, 1961, p. 1181.